Soil Dynamics and Earthquake Engineering 153 (2022) 107104

Contents lists available at ScienceDirect

Soil Dynamics and Earthquake Engineering

journal homepage: www.elsevier.com/locate/soildyn

Residential code-conforming structural seismic risk maps for Italy

Adriana Pacifico [a], Eugenio Chioccarelli [b,*], Iunio Iervolino [a]

[a] DIST, Dipartimento di Strutture per l'Ingegneria e l'Architettura, Università degli Studi di Napoli Federico II, Naples, Italy
[b] DICEAM, Dipartimento di Ingegneria Civile, dell'Energia, dell'Ambiente e dei Materiali, Università degli Studi Mediterranea di Reggio Calabria, Reggio Calabria, Italy

ARTICLE INFO

Keywords:
Failure rate
Fragility functions
Probabilistic seismic hazard analysis
Base-isolated buildings
Sequence-based hazard

ABSTRACT

RINTC – *Rischio Implicito delle strutture progettate secondo le NTC* is an Italian research project aiming at the evaluation of the seismic reliability inherent to design according to the current Italian building code. Within the project, different fixed-base residential and industrial structures typologies, as well as some base-isolated reinforced concrete buildings were addressed. The structures were located in three Italian sites characterized by different levels of seismic hazard. For each designed, modelled, and analyzed building, the seismic reliability, in term of annual failure rate, was computed. Based on these results, the aim of the study discussed in the paper is to derive national seismic risk maps for Italy in an ideal scenario where all the existing (residential) buildings would be code-conforming, either fixed-base or base-isolated. The analyses are performed at the municipality scale, combining the structural fragility functions with alternative models of probabilistic seismic hazard for Italy, and including exposure in terms of typological composition of the existing building stock. Results, presented in the form of maps of structural failure rates, generally show that: (i) despite the same return period of design seismic intensity over the country, failure rates greatly vary with the increasing hazard of the sites (generalizing one of the main outcomes of the RINTC project), (ii) the alternative hazard models produce limited variations of the failure rates, especially when global collapse is considered.

1. Introduction

The evolution of structural seismic design in Italy has been such that code improvements were mostly motivated by seismic events causing serious losses. The first document in which horizontal forces were considered for structural design goes back to 1909 and was referred to the geographic area affected by the magnitude (M) 7.1 Messina earthquake of 1908. In the following hundred years, a number of structural design codes were enacted, and the portion of national territory associated to seismic actions slowly increased (see Refs. [1,2] for a comprehensive analysis). The whole Italian territory has been considered seismically prone only since 2003 [3]. However, practitioners were not obliged to design according to the new hazard classification of the sites until 2008, when the current Italian building code, *Norme Tecniche per le Costruzioni* or NTC08 [4], was published. (An updated version of the Italian building code, NTC18 [5], was recently published but the hazard classification of the territory was not modified.) It can be considered at the state of the art internationally and is somewhat similar to Eurocode 8 [6]. In the code, the design seismic actions are derived from probabilistic seismic hazard analysis or PSHA (e.g. Ref. [7]) for the construction site.

Comparing the code evolution with the construction age of the Italian building portfolio, some infer that most of the existing buildings are expected to be designed with inadequate or absent seismic provisions (e.g., Ref. [8]) resulting in significant seismic vulnerability and risk (e.g. Ref. [9–12]). However, also the design according to current code exposes structures to some *implicit* seismic risk [13]. Moreover, the probability that a structure exceeds a defined performance (i.e., failure), in a given time interval, is not explicitly controlled by practitioners.

On this basis, in 2014, a large Italian national research project, *Rischio Implicito delle strutture progettate secondo le NTC* or RINTC [14,15], had the goal of quantifying the annual failure rate (numerically close to the annual failure probability) of code-conforming structures in Italy. Among others, residential fixed-based (FB) buildings considered in the project are reinforced concrete (RC) buildings of three, six and nine storeys (w/o infillings), and unreinforced masonry structures (URM) of two and three storeys. Moreover, residential six-storey RC base-isolated (BI) structures were also considered. The structures are supposedly located in three Italian sites chosen to be representative of different levels of design seismic hazard (low, medium, and high) according to the

* Corresponding author.
E-mail address: eugenio.chioccarelli@unirc.it (E. Chioccarelli).

https://doi.org/10.1016/j.soildyn.2021.107104
Received 4 August 2021; Received in revised form 16 November 2021; Accepted 25 November 2021

most recent probabilistic assessment [16]. Referring to each site and to specific soil conditions (to follow), each structure was first designed in accordance with NTC08 (or its 2018 update); then, the failure rate was computed with respect to ad-hoc defined performance levels. The results of the project showed that, although the design seismic actions (i.e., design ground motion intensity) have the same exceedance return period over the country, the structural reliability significantly changes across the sites. This is for reasons that further research showed attributable to inherent features of the code and of the seismic hazard of the considered sites beyond the exceedance return period of the seismic actions considered for design [17].

The aim of the work described herein is to depict the seismic risk in Italy in an ideal scenario where the existing (residential) buildings are substituted by the code-conforming structures of the RINTC project. To this end, the seismic risk is quantified, at the municipality scale, by the mean number of earthquakes that in one year cause structural failure of a randomly selected building of the municipality of interest; that is, still an annual failure rate leading to the annual expected number of buildings experiencing structural failure in the considered municipality. Thus, the failure rate must be a function of the seismic hazard of the site evaluated by means of PSHA (including the soil conditions), the seismic vulnerability of the structural typologies and the proportion among different structural typologies in the municipality, that is, the exposure.

Several maps of the municipality rates, which represent the result of the study, are derived based on different options for hazard and vulnerability characterization. In particular, three hazard models are considered: (i) the current official hazard for Italy, that is, the one on which design actions in the Italian code are based on (defined as MPS04 [16]); (ii) a more recent model, named MPS19, derived by a large research effort [18]; (iii) hazard computed via the so-called sequence--based PSHA or SPSHA [19], that also accounts for aftershocks' contribution, something neglected in classical hazard analysis (including both MPS04 and MPS19). As pertaining to structural vulnerability, a substitution criterion is defined to replace the existing residential buildings with fixed-base code-conforming URM and RC buildings, with different number of floors and architectural configurations. Moreover, an alternative scenario in which all the existing buildings are substituted by base-isolated six-storey RC buildings is considered.

The remainder of this paper is structured such that the buildings of RINTC project are described together with the fragility functions that are derived for the purposes of this study. Then, the methodology for the computation of the failure rates at municipality scale is presented. After introducing all the input models required for risk assessment, results considering four scenarios are discussed. The first two scenarios are those of PSHA based on MPS04 and combined with structural vulnerabilities of FB and BI structures. Then, results associated to PSHA based on MPS19 and structural vulnerability of FB structures are presented. Finally, the failure rates of FB structures are computed in the case of SPSHA, referring to MPS04. Some final remarks close the paper.

2. Fragility functions of code-conforming RINTC structures

In the RINTC project, a large set of residential buildings was designed according to the current Italian building code [4,5], to be ideally located in a few Italian sites: L'Aquila (AQ), Naples (NA), and Milan (MI), representative of high, medium, and low seismic hazard in the country, respectively. Different soil conditions were considered at the sites: soil class A (rock) and C (soft soil) according to the classification of the code. Each structure was designed referring to *damage* and *life-safety* limit states as defined in NTC08. On the other hand, structural reliability, was assessed in the project referring to two different performance levels (PL) that are named usability-preventing damage (UPD) and global collapse (GC). UPD is reached if one of following conditions occurs: (i) light damage in 50% of the main non-structural elements; (ii) at least one of the non-structural elements reaches a severe damage level leading to significant interruption of use; (iii) attainment of 95% of the maximum base-shear of the structure. GC, generally, corresponds to the displacement/deformation capacity associated to a 50% post-peak deterioration of the total base shear of the building (some adjustments of these criteria apply to specific typologies accounting for their peculiarities; see Refs. [13,20]).

In the RINTC project, for each building, multiple-stripes nonlinear dynamic analyses (MSA) [21] were performed on three-dimensional structural models at ten ground motion intensity measure (IM) levels (i.e., values), corresponding to ten exceedance return periods from 10^1 to 10^5 years. For each IM value, twenty two-component horizontal records were selected according to the conditional mean spectrum method [22]. In particular, each analysis was performed associating the two horizontal components of each record to the two main orthogonal directions of the structure and measuring the maximum response (i.e., in terms of either the roof displacement ratio or the maximum inter-storey drift ratio). The IM adopted for the MSA is the largest (between the two horizontal components) 5% damped pseudo-spectral acceleration at a period, T, close to the first vibration period of each model; it is indicated hereafter as $Sa(T)$.

In the following, the results of the dynamic analyses performed in the project are used to compute, for each structure (st) and for both the considered performance levels, the probability that PL is reached or exceeded given a value of IM, $P[PL^{(st)} \geq pl|im]$, that is the lognormal fragility function of the structure:

$$P\left[PL^{(st)} \geq pl|im\right] = \Phi\left[\frac{\ln(im) - \mu^{(st)}}{\sigma^{(st)}}\right], \tag{1}$$

where $\{\mu^{(st)}, \sigma^{(st)}\}$ are parameters retrieved via the R2R-software [23], neglecting estimation uncertainty [24]. In the following, the considered structures and their fragilities are described; further details are given in Ref. [25].

2.1. Reinforced-concrete structures

RC structures are moment resisting frame buildings of three (RC3) and six storeys (RC6) characterized by regularity in plan and elevation. While in the RINTC project bare-, pilotis-, and infilled-frames are designed, modelled, and analyzed [26] (Fig. 1), hereafter only the infilled configurations of three- and six-storey are considered; i.e., the most common configuration. Such structures are all designed for class C soil at the three sites. Fragility functions, modelled as per Eq. (1), refer to $Sa(0.15s)$ for the RC3 and $Sa(0.5s)$ for RC6. In Table 1, considered RC structures are listed and, for each of them, the parameters of fragility functions are reported for both performance levels.

In Fig. 2 the fragility functions are represented: black lines refer to GC and gray lines to UPD. (Although some IM values in the figure may appears unlikely, they are given to completely represent the curves and it should be noted that their effects on results of this study are negligible; see Section 5.1.)

2.2. Unreinforced masonry structures

For the three considered sites, two- and three-storey URM buildings (URM2 and URM3, respectively) made of perforated clay units with mortar joints were designed, modelled, and analyzed, within the RINTC project [27]. While buildings with both regular and irregular plan configurations were studied, here only those regular, according to the NTC08 criteria, are considered. They are characterized by different architectural configurations: the buildings associated to a letter E are examples of real modern URM buildings while those identified by a C (not to be confused with the soil class) are conceived as structural variations of regular wall arrangements. In both C and E classes, different thicknesses of structural walls are considered: C buildings are represented by six structural configurations from C1 to C5 and C7; E buildings are four, named as E2, E5, E8 and E9 (see Ref. [28] for further details).

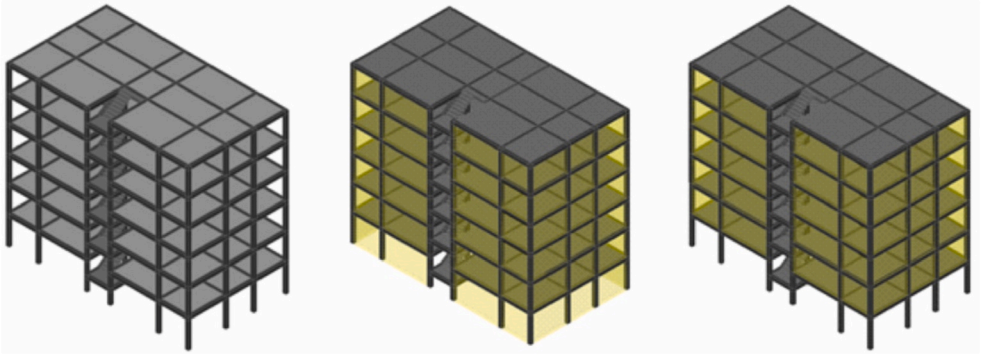

Fig. 1. RC6 buildings: bare-frame (left), infilled-frame (center); pilotis-frame (right) (Adapted from Ref. [14]).

Table 1
Parameters of RC fragility functions (*IM* in g).

Site	N. of storeys	UPD		GC	
		μ	σ	μ	σ
AQ	3	−0.44	0.41	1.79	0.66
AQ	6	−0.33	0.39	1.50	0.67
NA	3	−0.08	0.51	1.41	0.32
NA	6	−1.11	0.49	1.33	0.23
MI	3	0.06	0.51	0.30	0.32
MI	6	−0.55	0.29	0.40	0.31

Fig. 3 shows the different plan views of the URM structures considered herein. The two-storey building in L'Aquila has five alternative architectural configurations whereas, in the same site, three configurations for the three-storey building are considered. In Naples, the two-storey and three-storey building have two and four configurations, respectively. Finally, in Milan, three and four configurations are associated to the two-storey and three-storey building, respectively.

All the considered URM buildings were designed on class C soil (not to be confused with one of the configurations) apart from the three-storey buildings of L'Aquila for which design for C soil is not available; these cases (i.e., three architectural configurations) were substituted by the buildings designed on class A soil (the RINTC project

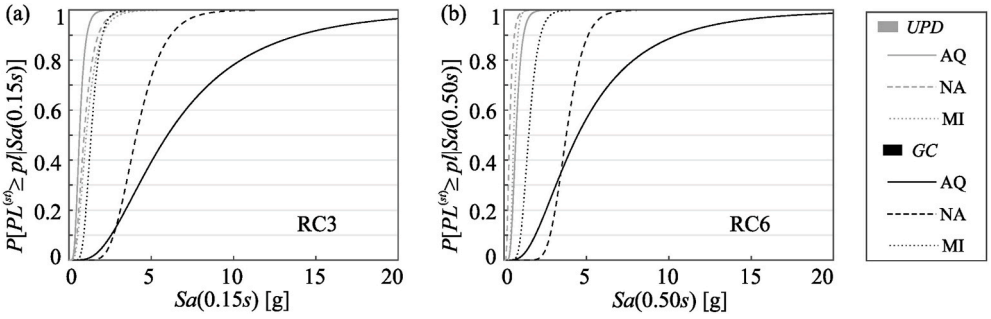

Fig. 2. Fragility functions of (a) RC3 and (b) RC6.

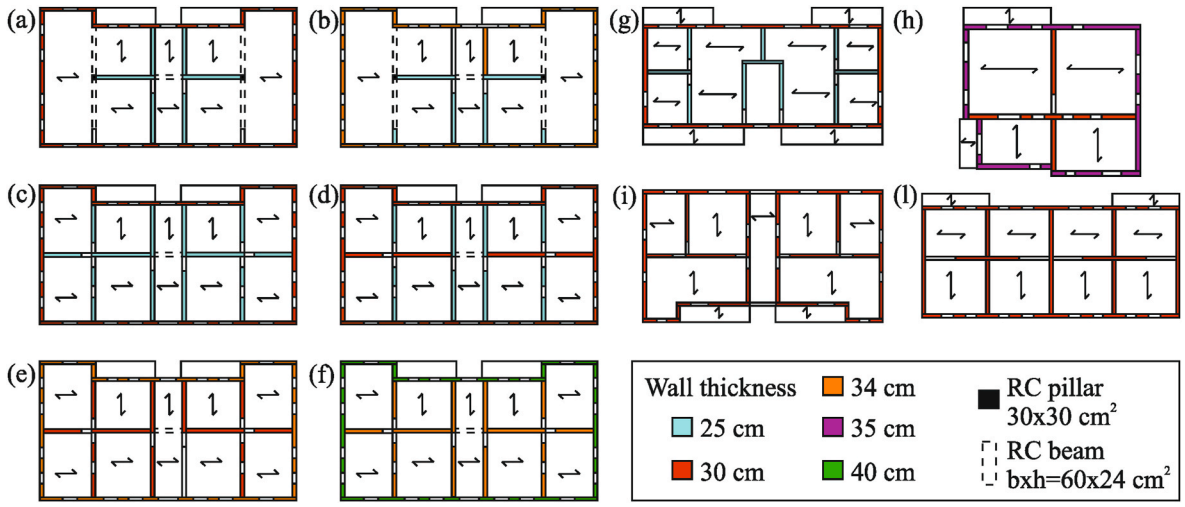

Fig. 3. Plan view of the URM buildings. Figures from (a)–(f) represent the C configurations (1–5 and 7 respectively), while figures from (g)–(l) represent the E configurations (2, 5 8 and 9 respectively).

has shown that the seismic vulnerability does not change dramatically with the soil class [13]).

Fragility functions are computed for each architectural configuration. Thus, considering the *k-th* architectural configuration pertaining to a given structural typology, the conditional failure probability, $P[PL^{(st,k)} \geq pl|im]$, is computed via Eq. (1). Then, the fragility function for each structural typology at a specific site, $P[PL^{(st)} \geq pl|im]$, is computed combining $P[PL^{(st,k)} \geq pl|im]$, as per Eq. (2):

$$P\left[PL^{(st)} \geq pl|im\right] = \sum_{k} P\left[PL^{(st,k)} \geq pl|im\right] \cdot w_{st,k}, \tag{2}$$

where $w_{st,k}$ weighs how much a specific architectural configuration is representative of the actual building portfolio (assuming that these configurations completely cover the building stock). Indeed, a value of $w_{st,k}$ was associated to each URM configuration basing on expert judgement (S. Cattari, personal communication) so that the sum of the weights for all the architectural configurations of the same structural typology equals to one.

The first vibration period of all the URM structures is close to 0.15*s*, thus the adopted *IM* for fragility functions is $Sa(0.15s)$. Table 2 shows, for each considered URM structure, the μ and σ parameters for both performance levels, along with the assigned $w_{st,k}$. Fig. 4 shows the URM fragilities.

2.3. Base-isolated structures

For the mid- and high-hazard sites, that is Naples and L'Aquila, respectively, residential six-storey infilled RC, base-isolated, buildings were also designed on class C soil. Indeed, it was assumed that BI structures are unlikely in low seismic hazard class. Three isolation systems were studied: (i) double-curvature friction pendulums (FPS); (ii) high-damping rubber bearings (HDRB); (iii) and hybrid system of HDRB and sliders (HDRB + Sld).

The UPD failure criteria are the same of RC FB structures, whereas GC needs to consider failure of both the isolation system and the superstructure. The superstructure failure criterion is the same of the RC buildings, while the failure of the base isolation was defined based on the specific device's responses described in Ref. [29].

For each isolation system, fragility functions were computed according to Eq. (1). The resulting curves at the same site were combined via Eq. (2) in which the alternative isolation systems were treated as the alternative architectural configurations of URM buildings. To this end, the weight of each isolation system was computed on the basis of the reconstruction data following the 2009 L'Aquila earthquake (M6.3); indeed, a large number of buildings were isolated with these three systems in the following percentages: 2% with HDRB, 41% FPS and 57% HDRB + Sld (D. Cardone, personal communication). Thus, the weights adopted in Eq. (2) are 0.02, 0.41 and 0.57, for HDRB, FPS and HDRB + Sld, respectively.

All the BI structures are characterized by first vibration periods close to 3*s*, thus the selected *IM* is $Sa(3.0s)$. Table 3 reports the fragility parameters for both performance levels together with the weight associated to each isolation system. In Fig. 5 the fragility functions of AQ and NA are represented.

Table 2
Parameters of URM fragility functions (*IM* in g).

Site	N. of storeys	Architectural configuration	$w_{st,k}$	UPD		GC	
				μ	σ	μ	σ
AQ	2	E2	0.20	−0.04	0.21	0.60	0.34
	2	E5	0.20	−0.32	0.26	0.56	0.43
	2	E8	0.20	−0.25	0.20	0.61	0.32
	2	E9	0.20	−0.11	0.18	0.28	0.26
	2	C3	0.20	−0.55	0.31	0.51	0.28
AQ	3	E2	0.33	−0.24	0.42	0.42	0.53
	3	E8	0.33	−0.26	0.38	0.47	0.51
	3	C1	0.33	−1.05	0.22	0.23	0.46
NA	2	C1	0.44	−0.72	0.24	0.95	0.42
	2	C4	0.56	−0.57	0.31	0.95	0.35
NA	3	E2	0.27	−0.06	0.57	0.88	0.24
	3	E8	0.27	−0.12	0.51	0.86	0.32
	3	C3	0.27	−0.87	0.28	0.69	0.45
	3	C5	0.20	−0.86	0.24	0.73	0.42
MI	2	E2	0.41	0.06	0.16	0.30	0.12
	2	C1	0.18	−1.16	0.09	0.45	0.08
	2	C7	0.41	−0.83	0.13	−0.18	0.08
MI	3	E2	0.27	−0.38	0.20	−0.41	0.08
	3	E8	0.27	−0.64	0.15	−0.39	0.13
	3	E9	0.27	−0.76	0.10	−0.63	0.094
	3	C2	0.18	−0.86	0.31	−0.06	0.12

3. Methodology for computation of failure rates

This section describes how fragility functions computed by the results of the RINTC project are used to derive ideal risk maps for Italy; i.e., assuming that all structures are code conforming. PSHA allows computing the rate of mainshocks (i.e., the maximum magnitude earthquake within each sequence) causing the exceedance of $IM = im$ for a known soil class, that is $\lambda_{E,im|\theta}$. The plot of $\lambda_{E,im|\theta}$ versus the possible *im* values is the so-called *hazard curve*. For a building of a given structural typology and located on a known soil class, the rate of mainshocks causing the building to fail, that is, to reach or exceed a performance level ($PL \geq pl$), $\lambda_{E,pl|st,\theta}$, can be computed via Eq. (3) in which it is assumed that the fragility is not dependent on the soil condition of the construction site and $\left|d\lambda_{E,im|\theta}(z)\right|$ is the absolute value of the differential of the hazard curve at $IM = z$:

$$\lambda_{E,pl|st,\theta} = \int_{im} P\left[PL^{(st)} \geq pl|z\right] \cdot \left|d\lambda_{E,im|\theta}(z)\right|. \tag{3}$$

If the site is representative of a municipality (e.g., the center of its area) and the fragility function represents the structural typology the building belongs to, Eq. (3) can be (approximately) applied to compute the failure rate of the buildings of the municipality belonging to the considered structural typology. The soil condition at the base of each building should be known, but usually this information is not available. However, it may be possible to compute $P[\theta_i]$, that is the probability that a generic building of the considered structural typology is located on each possible soil condition, *i*. Applying the total probability theorem, it results:

$$\lambda_{E,pl|st} = \sum_{i} \left\{ \int_{im} P\left[PL^{(st)} \geq pl|z\right] \cdot \left|d\lambda_{E,im|\theta_i}(z)\right| \right\} \cdot P[\theta_i]. \tag{4}$$

If the probability that a building of the municipality belongs to a given structural typology, $P[st]$, can also be computed, the rate of earthquakes causing the *generic* building (i.e., randomly selected) to reach or exceed a performance level, $\lambda_{E,pl}$, can be computed via Eq. (5), where it is assumed that soil condition and structural typology are independent random variables:

$$\lambda_{E,pl} = \sum_{st} \lambda_{E,pl|st} \cdot P[st] = \sum_{st} \sum_{i} \left\{ \int_{im} P\left[PL^{(st)} \geq pl|z\right] \cdot \left|d\lambda_{E,im|\theta_i}(z)\right| \right\} \cdot P[\theta_i] \cdot P[st]. \tag{5}$$

The rate computed in the previous equation is a risk metric that, with a probabilistically consistent approach, accounts for several sources of uncertainties related to: (i) earthquake source and propagation, (ii) soil site conditions, (iii) building structural typology, (iv) structural damage given ground motion intensity. Moreover, according to the classical hypotheses of performance-based earthquake engineering [30], $\lambda_{E,pl}$

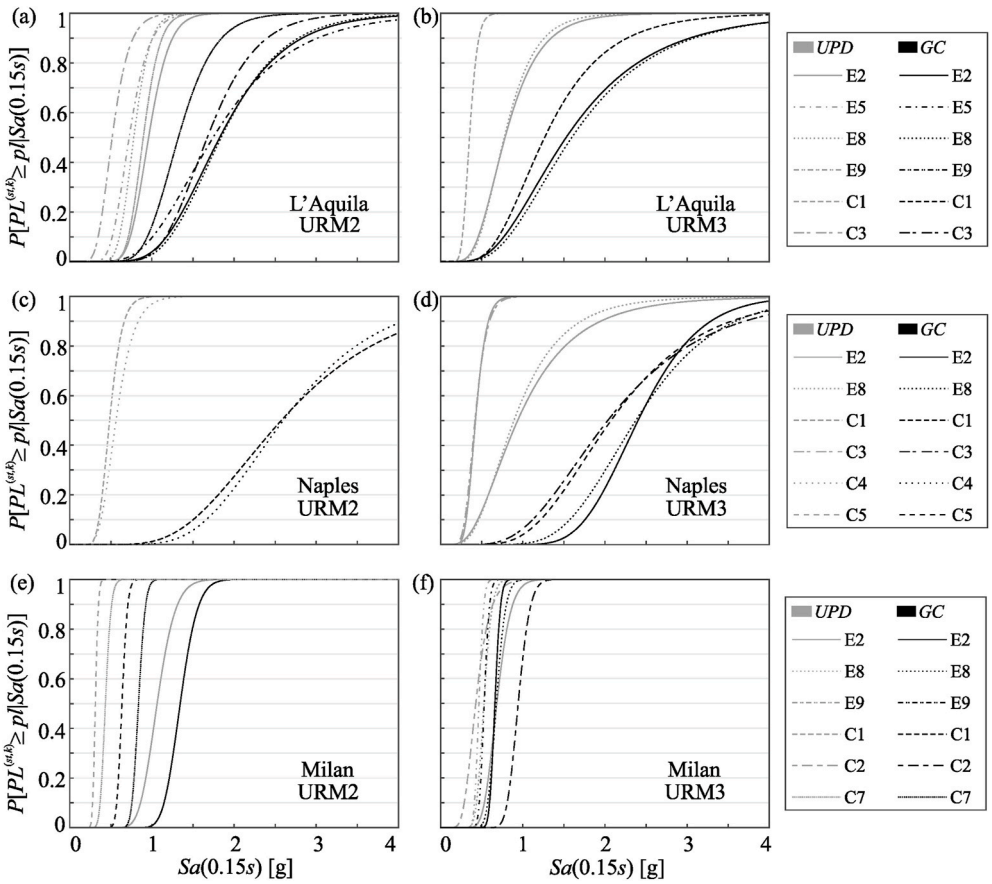

Fig. 4. Fragility functions of two storeys URM buildings (left column) of L'Aquila (top row), Naples (mid row), and Milan (bottom row) and of three storeys URM buildings of the same sites (right column).

Table 3
Parameters of BI fragility functions (*IM* in g).

Site	Isolation system	$w_{st,k}$	UPD		GC	
			μ	σ	μ	σ
L'Aquila	FPS	0.57	−1.51	0.37	−1.44	0.25
	HDRB	0.02	−1.77	0.44	−1.21	0.29
	HDRB + Sld	0.41	−1.55	0.35	−1.31	0.19
Naples	FPS	0.57	−1.43	0.18	−1.47	0.09
	HDRB	0.02	−1.54	0.17	−1.22	0.14
	HDRB + Sld	0.41	−1.61	0.2	−1.5	0.24

approximately leads to the expected number of failed buildings in the municipality in a small time interval $(t, t+\Delta t)$, $E[N_{pl}(t, t+\Delta t)]$:

$$E\left[N_{pl}(t, t+\Delta t)\right] \approx N_B \cdot \lambda_{E,pl} \cdot \Delta t, \tag{6}$$

in which N_B is the total number of buildings of the municipality. (The computed rate, practically, has not any other meaning that its use in this last equation, that is, to compute the expected value of damaged buildings.)

In fact, earthquakes are typically clustered in both time and space and, for each cluster, the mainshock is typically defined as the largest magnitude earthquake. Factually, PSHA neglects the hazard contribution of earthquakes preceding and following the mainshock within each cluster, that are identified as foreshocks and aftershocks, respectively. On the other hand, the so-called sequence-based PSHA, SPSHA [31], allows to quantify the seismic threat accounting for the effect of aftershocks in PSHA. SPSHA allows to compute the (annual) rate of mainshock-aftershocks sequences that cause at least one exceedance of the chosen *IM* threshold for the soil class and the site of interest, $\lambda_{im|\theta}$. Such a rate can be used to replace $\lambda_{E,im|\theta}$ in Eq. (5), so that it provides the rate of sequences causing the generic building to reach or exceed a

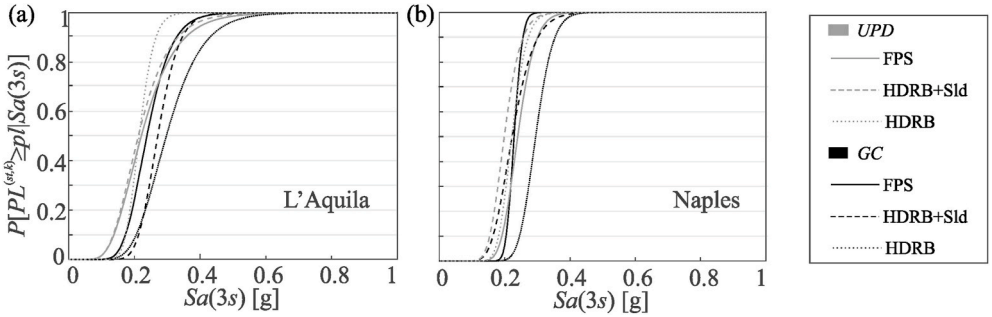

Fig. 5. Fragility functions of BI buildings of (a) L'Aquila and (b) Naples.

performance level, that is λ_{pl}. (In this context, seismic damage accumulation on the structures is neglected; see Ref. [32] for a discussion on this topic.)

4. Input data for nationwide code-conforming risk assessment

4.1. Probabilistic seismic hazard analyses based on MPS04

The current official probabilistic hazard assessment (also at the basis of the design seismic actions in the current Italian building code) considers thirty-six seismic source zones for the country (except Sardinia Island), as described in Ref. [33] (see Fig. 6b) and adopts a logic-tree constituted by sixteen branches [16]. Among them, the branch named 921, is the one adopted herein. Such a branch defines the seismicity of each seismic zone via the mean annual number of mainshocks per magnitude bins, the so-called *activity rates* (e.g. Ref. [19]), and requires the implementation of the ground motion prediction equation (GMPE) of [34]. The *IMs* for which PSHA is implemented here are the pseudo-spectral accelerations adopted for fragility functions, that is $T = \{0.15s,\ 0.5s,\ 3s\}$, and the peak ground acceleration, *PGA*. Being the 3s spectral period outside the definition range of the chosen GMPE, when such a period is of concern, the GMPE of [35] is adopted. (All these modelling choices are in accordance with the hazard evaluation involved in the record selections for nonlinear dynamic analyses in RINTC project.)

For each municipality, PSHA was performed according to the described models (i.e., reproducing branch 921 of the MPS04 model); the resulting hazard curves are identified hereafter as $\lambda^{04}_{E,im|\theta}$, to distinguish from results obtained when the MPS19 model is adopted; consequently, the failure rates are identified as $\lambda^{04}_{E,pl}$. Hazard analyses were performed via the REASSESS software [36]. An example of the hazard curves computed for each municipality is reported in Fig. 6a referring to *PGA* and rock soil conditions. In the same figure, the hazard curve computed for Milan, Naples, and L'Aquila are identified together with the exceedance rate corresponding to a return period (T_r) equal to 475 years (*yr*): this is a reference value for design of new structures and is also involved in the definition of the substitution criterion of existing structures discussed in the following section. Fig. 6b shows the seismic zones of [33], the location of the reference cities, and the values of *PGA* on rock corresponding, for each municipality, to $T_r = 475yr$, that is PGA_{475}. Both figures provide results of the PSHA for all the municipalities, except Sardinia (i.e., 337 municipalities) that, according to the source model, is outside the definition range of the GMPE.

4.2. Hazard classes and building replacement criteria

For the purposes of this work, RINTC data are incomplete in the sense that the studied sites and structural typologies cannot be directly representative of the whole Italian territory and building portfolio. Thus, some criteria to replace the existing buildings with the code-conforming structures from RINTC are adopted.

The Italian municipalities were first grouped in three arbitrarily defined hazard classes; i.e., high-, mid-, and low-hazard. The value of PGA_{475} of each municipality (Fig. 6b) was chosen for such a classification. The values of PGA_{475} (on A soil class, that is rock) of Naples (i.e., 0.15g) and Milan (0.05g) were taken as the limits of the classes, and sites characterized by a PGA_{475} lower than Milan were defined as low-hazard, sites with PGA_{475} lower than Naples (and larger than Milan) were considered a mid-hazard and sites with PGA_{475} larger than Naples were high-hazard. The resulting classification is represented in Fig. 6c: the municipalities in low-hazard class are about 16% of the total (excluding Sardinia), whereas those in mid- and high-hazard are about 47% and 36%, respectively.

Following such a classification, it was assumed that the RINTC buildings designed in L'Aquila, Naples, and Milan were representative of buildings designed in any municipality belonging to the high-, mid- and low-hazard class, respectively. It should be noted that, among the high hazard class, few Italian municipalities (259 over more than 8000) are characterized by PGA_{475} larger than the one computed for L'Aquila, that is, the fragilities associated to these sites were in fact computed for structures designed for a site with lower PGA_{475}.

Data on the existing residential building stock were retrieved by IRMA [37]. They include, for each municipality, the number of reinforced concrete and masonry buildings of one, two, three, or more than three storeys. To be able to substitute the existing building typologies with the available one, some simple criteria were adopted: the RC buildings with three storeys, or less, are substituted by RC3, while RC buildings with more than three storeys are substituted by RC6; the masonry buildings with one or two storeys are substituted by URM2, and the three-storey masonry buildings are substituted by URM3. Finally, masonry buildings with more than three storeys are substituted by RC6; i.e., assuming that new-design URM buildings with more than three storeys are unlikely.

The probability that a new building belongs to one of the considered structural typology, $P[st]$ from Eq. (7), where *st* corresponds to RC3, RC6, URM2, URM3, is computed as the number of buildings of that structural typology (N_{st}) divided by the total number of buildings in the considered municipality (N_{TOT}):

$$P[st] = \frac{N_{st}}{N_{TOT}}, \quad st = \{\text{RC3},\ \text{RC6},\ \text{URM2},\ \text{URM3}\}. \tag{7}$$

Fig. 7 shows, for each municipality and for each structural typology, the values of $P[st]$ after the application of the described substitution criterion. As shown, the probability associated to URM2 is, generally, the largest whereas the one associated to RC6 is the lowest. RC3 and

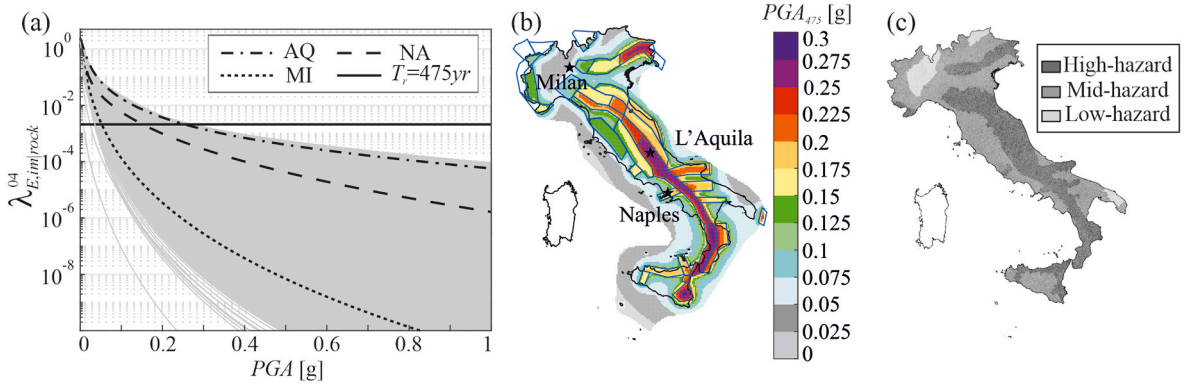

Fig. 6. (a) *PGA* hazard curves computed via PSHA for all the Italian municipalities adopting MPS04, (b) map of PGA_{475} (on rock) together with the thirty-six seismic zones of [33], (c) hazard classification according to PGA_{475} of each municipality.

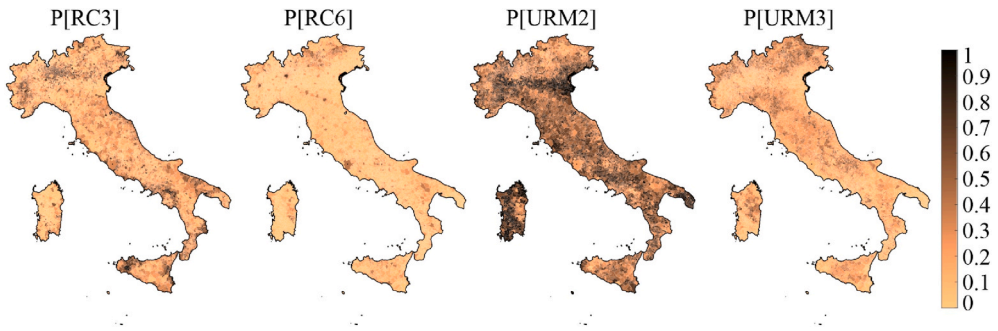

Fig. 7. Probability of each structural typology per municipality.

URM3 have non negligible probability with a scattered distribution over the country.

Regarding the substitution with code-conforming BI buildings, the analyses only refer to medium and high-hazard classes being, as previously mentioned, BI buildings considered unlikely for the low-hazard class. Moreover, according to the available fragilities (see Section 2), the substitution criterion is that each existing building, regardless the construction material or the number of the storeys, is replaced by a six-storey BI building.

4.3. Local soil classes at a municipality scale

In [38] it is provided a database of local soil characterizations for a grid of about one million points covering the whole Italian territory. For each point, the soil class (from A to D) according to NTC08 is defined. The latter can be converted into the soil classes of the GMPEs considered in the analyses. Indeed, both [34,35] GMPEs refer to three soil classes that are rock, stiff and soft soil. Soil conditions that, according to the Italian code, are identified as A correspond to the rock category, whereas soil conditions B correspond to stiff soil and soil conditions C and D correspond to soft soil class of the GMPEs.

To quantify the probability that the building of a given municipality is located on a specific soil class, required by Eq. (5), soil data can be combined with the data provided by the Italian *Istituto Nazionale di Statistica* (ISTAT) that identify the urbanized areas (see the *Data sources* section for further details) of each municipality, intended as the areas associated to city centers and built areas (other areas are classified as productive sites and sparse houses). More specifically, the grid of soil classes from Ref. [38] was superimposed to the map of the urbanized areas and, in each municipality, $P[\theta_i]$ was computed as the number of grid points of a given soil class, N_{θ_i}, dived by the total grid points within the urbanized areas, N_{urb}:

$$P[\theta_i] = \frac{N_{\theta_i}}{N_{urb}}, \quad \theta_i = \{rock, stiff, soft\}. \tag{8}$$

The resulting probabilities are reported in Fig. 8. The largest probabilities are associated to stiff soil in most of the municipalities; soft soil covers a non-negligible number of urbanized areas and is predominant in the north-eastern municipalities and along the coasts; finally, rock soil is significant only in a few areas (the effect on results of soil conditions is discussed in Ref. [39]).

4.4. Alternative hazard models

4.4.1. Probabilistic seismic hazard analyses based on MPS19

A recent hazard model for Italy, MPS19, was developed by a large community of researchers, led by the *Istituto Nazionale di Geofisica e Vulcanologia* (INGV) [18]. MPS19 entails a fairly complicated logic tree composed by about six-hundreds branches. To facilitate the reproducibility of the results, a weighted average grid-seismicity model was provided in Ref. [40]. It is a grid of about eleven thousand point-sources covering and surrounding the whole country. For each point of the grid, the mean annual number of earthquakes per magnitude bin (i.e., the activity rates) and a probabilistic distribution of the style-of-faulting is provided. In the following, the hazard curves computed via PSHA and based on the grid-seismicity model from MPS19, that is $\lambda^{19}_{E,im|\theta}$, will be used to compute the corresponding failure rates, $\lambda^{19}_{E,pl}$. It should be noted that, in this case, the adopted GMPE is that of [41], which entails a different definition of the *IM* with the respect to Ref. [34], adopted in MPS04. Indeed, the latter refers to the largest (horizontal) ground motion component, while the former provides the geometric mean of the two horizontal components. Since in RINTC project, fragility functions were derived in terms of the largest component, when MPS19 substitutes MPS04, [42] conversion was adopted to convert the hazard curves from geometric mean to largest component; this allows to consistently combine hazard results and fragility functions.

Moreover, due to the hazard modification, when $\lambda^{19}_{E,pl}$ is of concern, the substitution criteria described in Section 4.2 was re-applied in accordance with the new hazard results. Since the RINTC structures

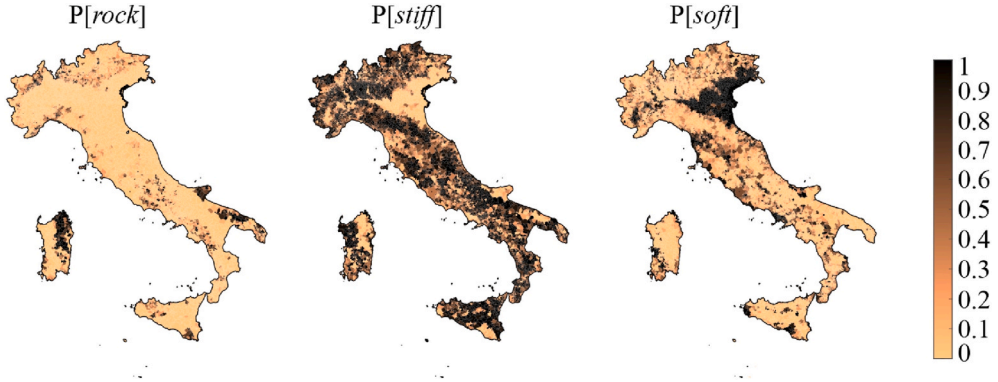

Fig. 8. Soil class probabilities in the urbanized areas of Italian municipalities.

were designed according to MPS04, the value of PGA_{475} of Naples and Milan, computed with MPS04, were maintained as limits of the hazard classes. The difference with respect to the previous case is that the value of PGA_{475} computed in each site and identifying its hazard class is derived by MPS19. The resulting classification is reported in Fig. 9a, which shows minor differences with respect to the equivalent classification of Fig. 6c. The percentage of municipalities classified as low-hazard reduces from 15% to 7% when the source model changes from MPS04 to MPS19; the number of the sites falling in the mid-hazard class increases from 48% to 65% while the sites associated to the high-hazard decrease from 37% to 28%. Fig. 9b shows the hazard curves in *PGA* (on rock) computed implementing MPS19 together with the hazard curves of L'Aquila, Naples, and Milan computed implementing MPS04 (in the legend AQ^{04}, NA^{04}, MI^{04}, respectively). The black horizontal line represents the 475 years exceedance return period (i.e., the one adopted for hazard classification). As shown, the hazard curves derived by the grid model are comparable with those from MPS04 in the range of low and medium return periods (i.e., up to about 500yr). Major differences appear when the return period increases. (It is also to note the systematic lower heterogeneity of the curves when passing from MPS04 to MPS19.)

4.4.2. Sequence-based probabilistic seismic hazard analyses based on MPS04

As early mentioned, SPSHA [31] includes the effect of aftershocks, along with that of mainshocks, in the hazard assessment. In Ref. [19] the hazard increments due to SPSHA with respect to PSHA were computed referring to the MPS04 source model, showing that, for a given return period, the value of the intensity measure computed via SPSHA (im_{SPSHA}) can be up to 30% larger than the corresponding value computed via PSHA (im_{PSHA}). Herein, still referring to the MPS04 source model, the SPSHA/PSHA comparison is extended to structural risk.

Because SPSHA requires a larger effort than PSHA, it was decided in this study – as an approximation – to perform SPSHA only for the site of L'Aquila, Naples, and Milan, to compute the hazard increases for these sites, and to adopt such increments to increase the PSHA hazard curves at the all the other Italian sites. Fig. 10a shows the hazard curves computed for L'Aquila, Naples, and Milan on rock site conditions and considering the spectral ordinates of interest for the structural typologies, that is $Sa(0.15s)$ and $Sa(0.5s)$ (the models here adopted for SPSHA are the same described in Ref. [19]). Then, for each site and spectral ordinate, the hazard increments with respect to PSHA, that is the im_{SPSHA}/im_{PSHA} ratio, was computed as a function of the return period; see Fig. 10b (the ratios computed at given site, considering different spectral periods, may intersect; see Ref. [19]). The hazard increments computed in L'Aquila, Naples, and Milan were used to scale the corresponding hazard results computed for the municipalities in high-, medium-, and low-hazard class, respectively. The resulting hazard curves are used to compare the failure rates considering the effect of aftershocks with those considering mainshocks only (see the following sections).

5. Results and discussions

5.1. Seismic risk for fixed-base structures based on MPS04 hazard

This section discusses the results of Eq. (5) when the hazard curves are computed via PSHA based on MPS04 and in the hypothesis of substituting the existing residential buildings with the FB code-conforming ones. Fig. 11a represents the failure rates of each Italian municipality considering UPD ($\lambda^{04}_{E,UPD}$), whereas Fig. 11b refers to GC ($\lambda^{04}_{E,GC}$). It is worth noting that, hereafter, failure rates lower than 1E-05 are substituted by 1E-05 to avoid significant extrapolations of hazard and fragility models, acknowledging the approach of [13]. This value was chosen based on the maximum return period at which MSA is performed (see Section 2).

UPD annual failure rates vary between 1E-05 to 6.62E-03 and 51% of the municipalities are characterized by rates larger than 1E-03; 30% of sites have rates within 1E-04 and 1E-03; about the 20% of municipalities have rates lower than 1E-04. A comparison between Figs. 11a and 6c shows the effect on results of the hazard classes. More in details, all the sites belonging to the low hazard class show $\lambda^{04}_{E,UPD}$ lower than 5E-05, whereas 95% of the municipalities in the high hazard class have rates higher than 1E-03.

GC annual failure rates range between 1E-05 and 8.91E-04. Most of the sites (64%) presents a failure rate lower than 5E-05 and values higher than 5E-05 are associated to the municipalities belonging to high-hazard regions. The largest failure rates are computed in municipalities of central and southern Apennines, reflecting the hazard of the region. With respect to UPD, GC failure rates are up to two orders of magnitude lower as shown by the map of ratios, $\lambda^{04}_{E,UPD}/\lambda^{04}_{E,GC}$, reported in Fig. 11c. In 60% and 8% of the municipalities the ratio is between 1E+01 and 1E+02, and higher than 1E+02, respectively. For the remaining 32% of the sites, the same order of magnitude for the two failure rates is computed; results in these sites are controlled by the lower bound of 1E-05.

5.2. Alternative risk metric

The hypotheses characterizing the ideal scenarios discussed in this study are not available in literature and a comparison of the results of this work with other similar studies is not directly possible. However, it may be useful to provide risk maps in a comparable representation with respect to available studies dealing with the national seismic risk of existing structures. These risk maps are often presented in two scales (e.g., Refs. [10,12]): (i) the percentage and (ii) the absolute number of failed buildings per municipality in a given time interval (usually, one year). Thus, it should be noted that, in accordance with Eq. (6), all the

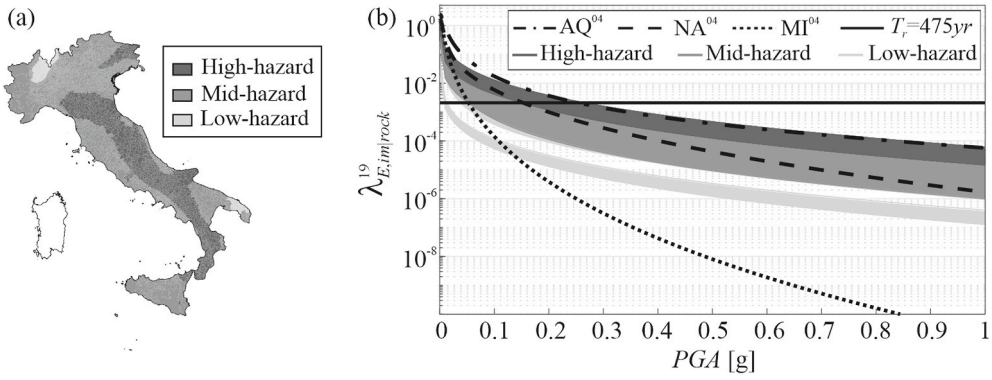

Fig. 9. (a) Hazard classification of the Italian municipalities according to MPS19; (b) *PGA* hazard curves computed via PSHA adopting MPS19.

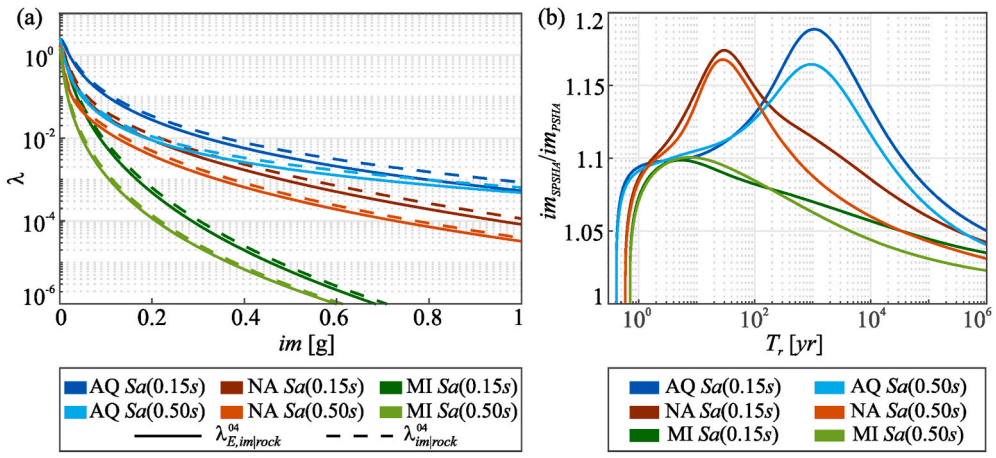

Fig. 10. (a) Hazard curves of the three considered sites in term of $Sa(0.15s)$ and $Sa(0.5s)$ evaluated with PSHA (continuous lines) or SPSHA (dashed lines); (b) hazard increments due to SPSHA with respect to PSHA.

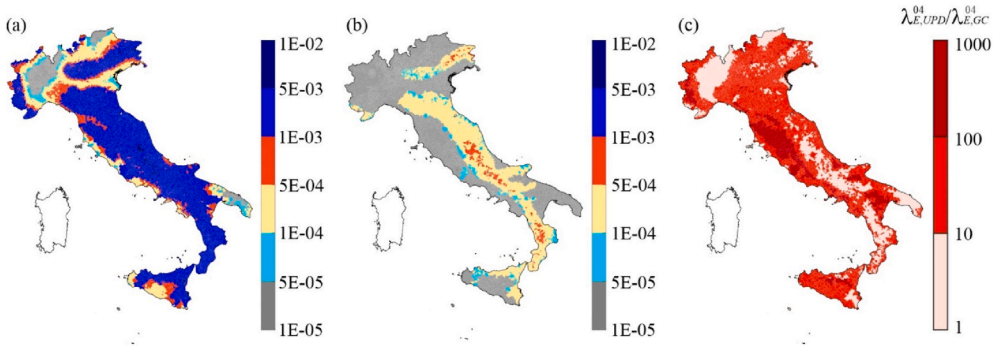

Fig. 11. Maps of failure rates per municipalities considering (a) UPD and (b) GC evaluated adopting MPS04 and considering FB structures; (c) map of the ratios of the failure rates evaluated for UPD and GC.

maps of failure rates shown here can also be interpreted as maps of the annual number of failed buildings in each municipality divided by the total number of buildings of the same municipality. Moreover, the rates in Fig. 11 are also converted into the mean annual number of failed buildings per municipality, that is, from Eq. (6) assuming Δt equal to one year, see Fig. 12.

When the UPD performance level is considered, Fig. 12a, for the 26% of the municipality the expected value of failed building is lower than 0.1, it ranges between 0.1 and 1 for the 32% of municipalities whereas it is between 1 and 5 for the 34% of the municipalities; finally, the expected number of failed buildings is larger than 5 in 8% of the municipalities. Fig. 12b presents the expected value of buildings at GC. In most of the municipalities (73%), the expected number of failed buildings ranges between 0 and 0.1. Among the remaining municipalities, that mostly belong to the high-hazard class, this expected number ranges between 1 and 5 in 26% of the considered sites, and it is larger than 5 only in 1% of the municipalities.

5.3. Seismic risk for base-isolated structures based on MPS04

This section discusses the case in which all the existing buildings (except those in the low-hazard class) are replaced with RC BI structures;

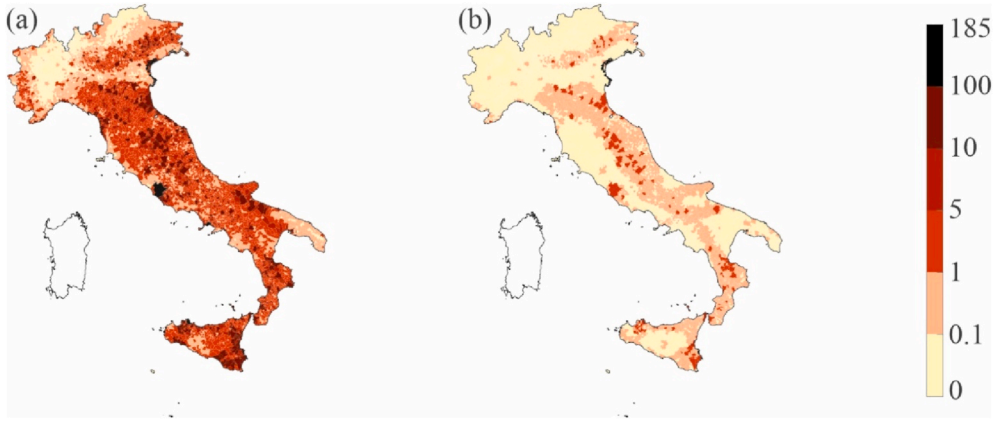

Fig. 12. Maps of the expected number of failed buildings in one year per municipality considering (a) UPD and (b) GC.

seismic hazard is evaluated via PSHA based on MPS04. The resulting maps of failure rates for UPD and GC are reported in Fig. 13a and Fig. 13b, respectively. As shown, the two maps are similar; this is because UPD refers to the response of superstructure that is typically not affected by damages as long as the isolation system does not fail. However, the failure of the isolation system corresponds to GC. Only for UPD, few municipalities (0.38%) have failure rates larger than 5E-04; for both performance levels, more than 70% of the municipalities have rates lower than 5E-05.

In Fig. 14, the two alternative substitution criteria are compared providing, for each municipality, the ratio between the values of the failure rates related to BI and FB structures; UPD and GC are considered in Fig. 14a and b, respectively. Reddish color is assigned when the failure rate associated to BI structures is larger than the one computed for FB structures; green is the opposite case. When comparison refers to UPD, 100% of sites are green: failure rates for BI structures are one and two orders of magnitude lower than FB structures for 67% and 23% of the sites, respectively. For GC, the failure rate associated to the FB structures are larger than those associated to the BI structures for 85% of the municipalities. On the other hand, in 15% of the sites, GC rates for BI are larger than FB and the ratio of failure rates is between 1 and 10, whereas such a rate is larger than 10 only for 0.2% of the cases. These results, although possibly counterintuitive, are in accordance with the findings of other studies (e.g., Refs. [43,44]).

5.4. Seismic risk for fixed-base structures based on MPS19

In this section, the results of Eq. (5) when hazard curves are computed via PSHA based on MPS19 and considering FB code-conforming buildings, are discussed. When UPD is concerned, the annual failure rates range from 1E-05 to 8.1E-03. Less than the 0.1% of the municipalities have UPD failure rates lower than 1E-04; in the 39% of the sites, mostly belonging to the low-seismicity class, they are from 1E-04 to 1E-03, whereas, in most of the sites, (61%) failure rates are larger than 1E-03. As regards GC failure rates, they are between 1E-05 in 1.3E-03; the largest values are in north-eastern and central Italy.

The discussed results are also presented in the form of maps of the ratios between failure rates based on MPS19 and those based on MPS04. Fig. 15c refers to UPD ($\lambda^{19}_{E,UPD}/\lambda^{04}_{E,UPD}$), whereas Fig. 15d refers to GC ($\lambda^{19}_{E,GC}/\lambda^{04}_{E,GC}$). In both figures, reddish color is adopted for the cases in which MPS19 produces failure rates larger than MPS04, green otherwise. For UPD, most of the case, that is 87% of the municipalities, show failure rates resulting from the two source models of the same order of magnitude. MPS19 provides failure rates one order of magnitude larger than MPS04 in the low hazard class of the Northern Italy and in few sites of the Po Valley and Sicily (i.e., 13% of the sites). Overall, UPD failure rates from MPS19 are larger than MPS04 for the 72% of the Italian municipality (excluding Sardinia); such sites correspond, mostly, to the low and medium hazard classes, according to MPS04. Conversely, in the 28% of sites, mostly belonging to the high-hazard class, MPS19 provides UPD failure rates lower than MPS04. As regards GC, Fig. 15b shows that failure rates are of the same order of magnitude regardless the adopted source model in the 94% of the municipalities. In 84% of sites, the MPS19 failure rates are larger than the MPS04; in the remaining 16% of sites, mostly located along the Apennines and in Sicily, MPS19 rates are lower than MPS04.

5.5. Seismic risk for fixed-base structures accounting for mainshocks-aftershocks contribution to the hazard

This section discusses the risk assessment when the contribution of mainshock-aftershocks sequences is considered via SPSHA based on MPS04. The failure rates are computed referring to UPD and GC, that is λ^{04}_{UPD} and λ^{04}_{GC}. Fig. 16 shows results, for each municipality, in term of comparison with respect to those from PSHA (Fig. 11). As expected, all the ratios are larger than one: UPD ratios varies between 1.25 and 1.50 in most of the municipalities (89%); all the values lower than 1.25 are associated to municipalities (10% of the total) belonging to the low-hazard class whereas in the 1% of the municipalities, all belonging to the high-hazard class, ratios are higher than 1.50 (up to 1.60). For GC, the ratios increase up to almost 1.80. In the low-hazard class and in most of the mid-hazard class, the ratios of the failure rates are between 1.0 and 1.25, (58% of the Italian municipalities). They are between 1.25 and 1.50 in 17% of the sites that correspond to the Calabrian Arc and some municipalities of the northeastern Italy. In the other municipalities, all belonging to the high-hazard class, the ratios vary between 1.50 and 1.80. In conclusion, the aftershocks' effect to the seismic hazard may almost double the GC failure rates.

6. Conclusions

This study herein presented evaluated the ideal seismic risk of Italy at municipality scale; i.e., assuming that all the residential buildings are replaced with code-conforming structures. For each municipality, the risk is quantified via the mean number of mainshocks (or mainshock-aftershocks seismic sequences), that in one year, cause failure of a randomly selected building of the municipality of interest. Considered structural performances are usability-preventing damage (UPD) and global collapse (GC). Structures designed, modelled, and analyzed in the RINTC project for three Italian sites (i.e., L'Aquila, Naples, and Milan), were adopted to represent code-conforming buildings of the

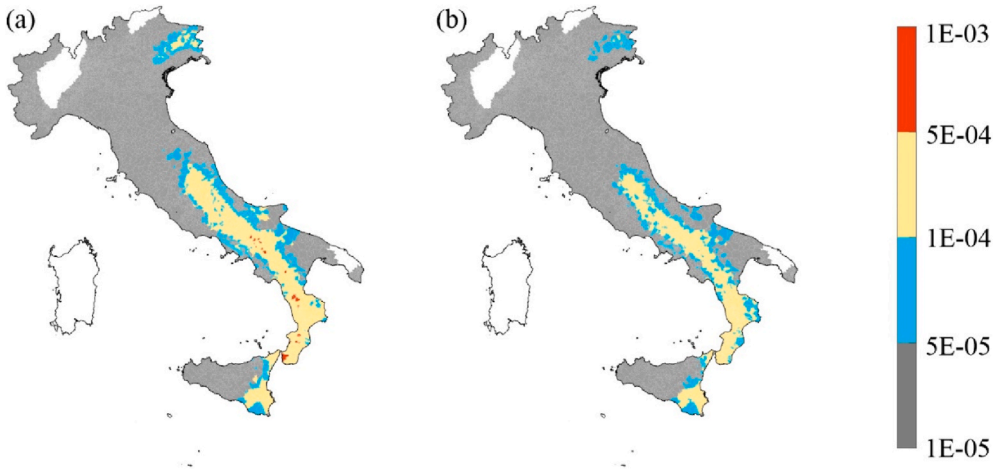

Fig. 13. Maps of failure rates per municipalities considering (a) UPD and (b) GC evaluated adopting MPS04 source model and considering BI structures.

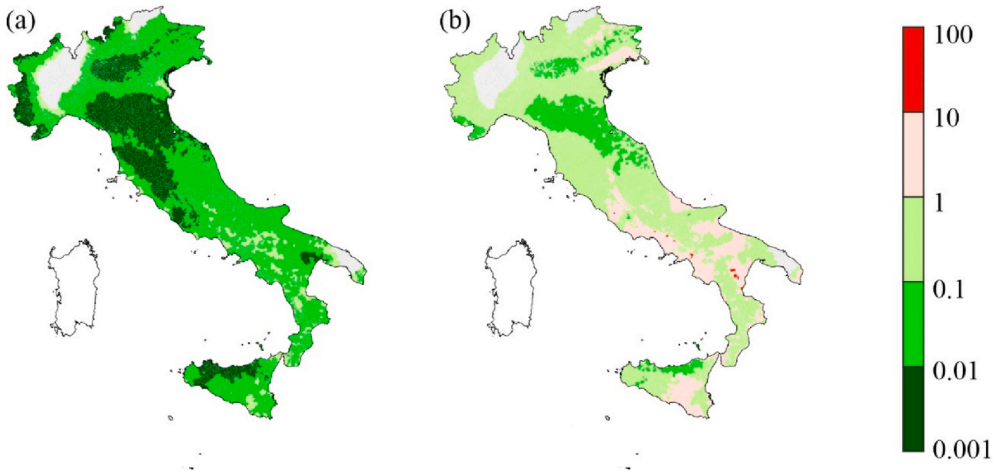

Fig. 14. Ratio of the failure rates computed for BI and FB structures: (a) UPD, and (b) GC.

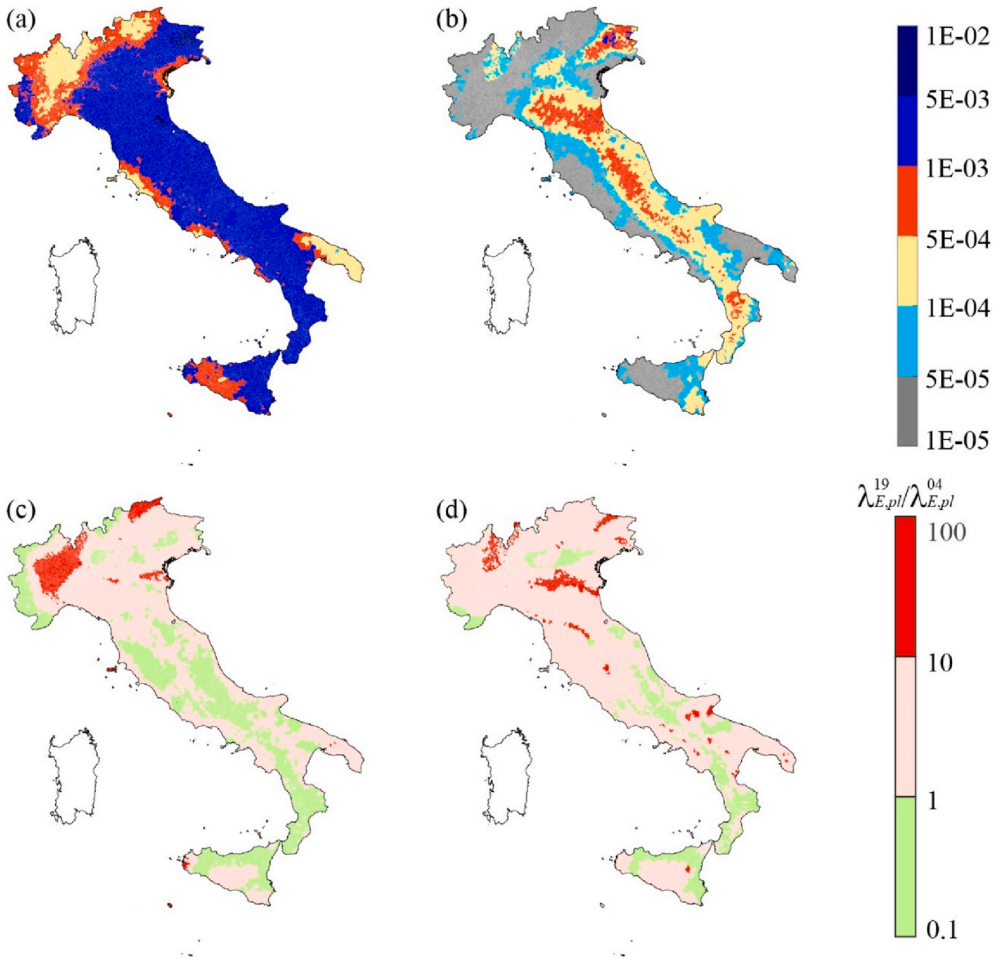

Fig. 15. Maps of failure rates per municipalities considering (a) UPD and (b) GC evaluated adopting MPS19 source model; map of the ratios of the failure rates computed according to MPS19 and MPS04: (c) UPD and (d) GC.

municipalities in high-, mid- and low-seismic hazard classes, respectively. These classes were identified according to the value of the PGA_{475} (on rock) computed for each Italian municipality. Different risk modelling options were considered, and the main conclusions from them are listed hereunder.

- When PSHA is based on the current reference Italian hazard model (MPS04) and fixed-base buildings are considered, it is shown that, although the design actions are characterized by the same exceedance probability, the failure rates are largely different among different structural typologies and sites. This generalizes the results of the RINTC project. UPD failure rates, over the country, vary between 1E-05 and 6.62E-03; 51% of the municipalities are

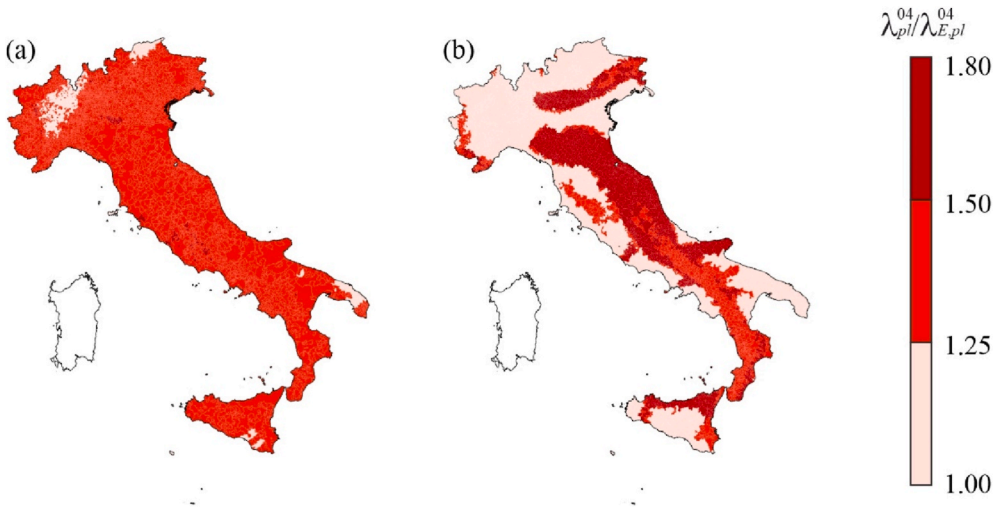

Fig. 16. Ratio of the failure rates computed via SPSHA and PSHA: (a) UPD and (b) GC.

characterized by failure rates larger than 1E-03 while all the others are lower. Referring to the GC, failure rates range from 1E-05 to 8.91E-04 and the most of Italian municipalities (64%) shows a failure rate lower than 5E-05. The replacement criterion was proven to be significant for such results; indeed, failure rates show relatively low variability within each seismic hazard class. In terms of annual expected number of failed buildings per municipality, the results show that, in most of the sites (i.e., 34%), the number of buildings expected to exceed UPD is between 0.1 and 1. For GC, the expected number of failed building ranges between 0.1 and 1 at 73% of the Italian municipalities.

- Considering base-isolated buildings replacing all the existing structures, with MPS04 hazard, the UPD and GC failure rates are comparable in each Italian municipality. As expected, they are lower than the counterpart computed for FB structures. This happens at 100% of sites for UPD, for which rates differ of one or two orders of magnitude. In the case of GC, it occurs at 85% of the sites whereas, in the remaining 15%, BI structures provide larger rates than FB.
- When PSHA is based on a recent Italian hazard model (MPS19) the UPD risk of FB code-conforming buildings shows that failure rates are higher than those due to MPS04 at 72% of the municipalities (mostly corresponding to the low-, mid-seismic hazard classes). Such a percentage increases to 84% of the sites in the case of GC failure rates.
- When the effect of mainshock-aftershocks sequences is considered (i.e., in the case of SPSHA based on MPS04) the SPSHA/PSHA ratios of UPD failure rates for FB buildings vary from 1.25 to 1.50 in 89% of the municipalities. The analogous ratios, in the GC case, reach 1.80 in high-hazard regions.

It must be finally remarked that all the results herein presented follow some (arbitrary) choices made for the hazard and the vulnerability characterization. Moreover, the limited available information lead to assume stochastic independency between soil conditions and structural typologies and the definition of substitution criteria based on the hazard classification of the Italian municipalities. Nevertheless, the provided maps may help to provide insights on the seismic risk in Italy inherent to the current building code.

Credit author statement

Contributor Roles Taxonomy Statement.

According Elsevier's sample CRediT statement, the authors of the aforementioned manuscript had the following roles during development of the scientific work.

Adriana Pacifico: Software, Validation, Writing - Original Draft.

Eugenio Chioccarelli: Methodology, Validation, Writing - Review & Editing.

Iunio Iervolino: Conceptualization, Methodology, Writing - Review & Editing.

Data sources

In addition to the cited references, data used in this study were accessible from the following source (last accessed August 03, 2021): *Istituto Nazionale di Statistica* (ISTAT) (https://www.istat.it/it/archivio/222527).

Declaration of competing interest

The authors declare that they have no known competing financial interests or personal relationships that could have appeared to influence the work reported in this paper.

Acknowledgements

The study presented in this article was developed within the activities of the ReLUIS-DPC 2019–2021 research programs, funded by the Presidenza del Consiglio dei Ministri— Dipartimento della Protezione Civile (DPC). Note that the opinions and conclusions presented by the authors do not necessarily reflect those of the funding entity.

References

[1] Di Pasquale G, Fralleone A, Pizza AG, Serra C. Relevant changes to the Italian seismic Code from 1909 to 1975 – a synoptic table. De Marco, Martini (eds) La classificazione e la normative sismica italiana dal 1909 al 1984. Roma: Istituto Poligrafico e Zecca dello Stato; 1999 (in Italian).

[2] Di Pasquale G, Fralleone A, Pizza AG, Serra C. Synthesis of the code evolution from the Royal decree issued after the Messina and Reggio earthquake up to the first Ministry decree issued after the law n.64/74. In: De Marco, Martini (eds) La classificazione e la normative sismica italiana dal 1909 al 1984. Roma: Istituto Poligrafico e Zecca dello Stato; 1999 (in Italian).

[3] OPCM 3274. Primi elementi in materia di criteri generali per la classificazione sismica del territorio nazionale e di normative tecniche per le costruzioni in zona sismica. G.U. della Repubblica Italiana n.105 2003 (in Italian).

[4] CS.LL.PP. Decreto Ministeriale del 14/1/2008, Norme tecniche per le costruzioni. G.U. della Repubblica Italiana n.29; 2008 (in Italian).

[5] CS.LL.PP.. Decreto Ministeriale del 17/1/2018, Aggiornamento delle "Norme tecniche per le costruzioni. G.U. della Repubblica Italiana n.42 2018 (in Italian).

[6] CEN, European Committee for Standardization TC250/SC8/(2003) Eurocode 8: Design provisions for earthquake resistance of structures. Part 1.1 general rules, seismic actions and rules for buildings 2004. PrEN1998-1.

[7] McGuire RK. Seismic hazard and risk analysis. MNO-10. Oakland, CA: Earthquake Engineering Research Institute; 2004.

[8] Petruzzelli F, Iervolino I. NODE: a large-scale seismic risk prioritization tool for Italy based on nominal structural performance. Bull Earthq Eng 2021;19:2763–96. https://doi.org/10.1007/s10518-021-01093-1.
[9] Corbane C, Hancilar U, Ehrlich D, De Groeve T. Pan-European seismic risk assessment: a proof of concept using the earthquake loss estimation routine (ELER). Bull Earthq Eng 2017;15:1057–83. https://doi.org/10.1007/s10518-016-9993-5.
[10] Crowley H, Colombi M, Borzi B, Faravelli M, Onida M, Lopez M, et al. A comparison of seismic risk maps for Italy. Bull Earthq Eng 2009;7:149–80. https://doi.org/10.1007/s10518-008-9100-7.
[11] Crowley H, Despotaki V, Silva V, Dabbeek J, Romão X, Pereira N, et al. Model of seismic design lateral force levels for the existing reinforced concrete European building stock. Bull Earthq Eng 2021;19:2839–65. https://doi.org/10.1007/s10518-021-01083-3.
[12] Dolce M, Prota A, Borzi B, da Porto F, Lagomarsino S, Magenes G, et al. Seismic risk assessment of residential buildings in Italy. Bull Earthquake Eng 2021;19:2999–3032. https://doi.org/10.1007/s10518-020-01009-5.
[13] Iervolino I, Spillatura A, Bazzurro P. Seismic reliability of code-conforming Italian buildings. J Earthq Eng 2018;22:5–27. https://doi.org/10.1080/13632469.2018.1540372 Seismic.
[14] RINTC-Workgroup. Results of the 2015-2018. The iplicit risk of code-conforming structures in Italy (RINTC) project. ReLUIS report. Naples, Italy: Rete dei Laboratori Universitari di Ingegneria Sismica; 2018. Available at: http://www.reluis.it.
[15] Iervolino I, Dolce M. Foreword to the special issue for the RINTC (the implicit seismic risk of code-conforming structures) project. J Earthq Eng 2018;22:1–4. https://doi.org/10.1080/13632469.2018.1543697.
[16] Stucchi M, Meletti C, Montaldo V, Crowley H, Calvi GM, Boschi E. Seismic hazard assessment (2003-2009) for the Italian building code. Bull Seismol Soc Am 2011;101:1885–911. https://doi.org/10.1785/0120100130.
[17] Cito P, Iervolino I. Peak-over-threshold: quantifying ground motion beyond design. Earthq Eng Struct Dynam 2020;49:458–78. https://doi.org/10.1002/eqe.3248.
[18] Meletti C, Marzocchi W, D'Amico V, Lanzano G, Luzi L, Martinelli F, et al. The new Italian seismic hazard model (MPS19). Ann Geophys 2021;64. https://doi.org/10.4401/ag-8579.
[19] Iervolino I, Chioccarelli E, Giorgio M. Aftershocks' effect on structural design actions in Italy. Bull Seismol Soc Am 2018;108:2209–20. https://doi.org/10.1785/0120170339.
[20] Suzuki A, Iervolino I. Seismic fragility of code-conforming Italian buildings based on SDoF approximation. J Earthq Eng 2021;25(14):2873–907. https://doi.org/10.1080/13632469.2019.1657989.
[21] Jalayer F, Cornell CA. Measuring bias in structural response caused by ground motion scaling. Earthq Eng Struct Dynam 2009;38:951–72. https://doi.org/10.1002/eqe.876.
[22] Lin T, Haselton CB, Baker JW. Conditional spectrum-based ground motion selection. Part I: hazard consistency for risk-based assessments. Earthq Eng Struct Dynam 2013;42:1847–65. https://doi.org/10.1002/eqe.2301.
[23] Baraschino R, Baltzopoulos G, Iervolino I. R2R-EU: software for fragility fitting and evaluation of estimation uncertainty in seismic risk analysis. Soil Dynam Earthq Eng 2020;132. https://doi.org/10.1016/j.soildyn.2020.106093.
[24] Iervolino I. Assessing uncertainty in estimation of seismic response for PBEE. Earthq Eng Struct Dynam 2017;46:1711–23. https://doi.org/10.1002/eqe.2883.
[25] Iervolino I, Baraschino R, Cardone D, Della Corte G, Lagomarsino S, Penna A, et al. Seismic fragility of Italian code-conforming buildings by multi-stripe dynamic analysis of three-dimensional structural models [submitted for pubblication]. 2021.
[26] Ricci P, Manfredi V, Noto F, Terrenzi M, Petrone C, Celano F, et al. Modeling and seismic response analysis of Italian code-conforming reinforced concrete buildings. J Earthq Eng 2018;22:105–39. https://doi.org/10.1080/13632469.2018.1527733.
[27] Cattari S, Camilletti D, Lagomarsino S, Bracchi S, Rota M, Penna A. Masonry Italian code-conforming buildings. Part 2: nonlinear modelling and time-history analysis. J Earthq Eng 2018;22:2010–40. https://doi.org/10.1080/13632469.2018.1541030.
[28] Manzini CF, Magenes G, Penna A, da Porto F, Camilletti D, Cattari S, et al. Masonry Italian code-conforming buildings. Part 1: case studies and design methods. J Earthq Eng 2018;22:54–73. https://doi.org/10.1080/13632469.2018.1532358.
[29] Ragni L, Cardone D, Conte N, Dall'Asta A, Di Cesare A, Flora A, et al. Modelling and seismic response analysis of Italian code-conforming base-isolated buildings. J Earthq Eng 2018;22:198–230. https://doi.org/10.1080/13632469.2018.1527263.
[30] Cornell CA, Krawinkler H. Progress and challenges in seismic performance assessment. PEER Cent News 2000;3. https://apps.peer.berkeley.edu/news/2000spring/ind.
[31] Iervolino I, Giorgio M, Polidoro B. Sequence-based probabilistic seismic hazard analysis. Bull Seismol Soc Am 2014;104:1006–12. https://doi.org/10.1785/0120130207.
[32] Iervolino I, Chioccarelli E, Suzuki A. Seismic damage accumulation in multiple mainshock-aftershock sequences. Earthq Eng Struct Dynam 2020;49:1007–27. https://doi.org/10.1002/eqe.3275.
[33] Meletti C, Galadini F, Valensise G, Stucchi M, Basili R, Barba S, et al. A seismic source zone model for the seismic hazard assessment of the Italian territory. Tectonophysics 2008;450(1–4):85–108. https://doi.org/10.1016/j.tecto.2008.01.003.
[34] Ambraseys NN, Simpson KA, Bommer JJ. Prediction of horizontal response spectra in Europe. Earthq Eng Struct Dynam 1996;25(4):371–400. https://doi.org/10.1002/(SICI)1096-9845(199604)25:4<371::AID-EQE550>3.0.CO;2-A.
[35] Akkar S, Bommer JJ. Empirical equations for the prediction of PGA, PGV, and spectral accelerations in Europe, the mediterranean region, and the Middle East. Seismol Res Lett 2010;81:195–206. https://doi.org/10.1785/gssrl.81.2.195.
[36] Chioccarelli E, Cito P, Iervolino I, Giorgio M. Reassess V2.0: software for single- and multi-site probabilistic seismic hazard analysis. Bull Earthq Eng 2019;17:1769–93. https://doi.org/10.1007/s10518-018-00531-x.
[37] Borzi B, Onida M, Faravelli M, Polli D, Pagano M, Quaroni D, et al. IRMA platform for the calculation of damages and risks of Italian residential buildings. Bull Earthq Eng 2020;19:3033–55. https://doi.org/10.1007/s10518-020-00924-x.
[38] Forte G, Chioccarelli E, De Falco M, Cito P, Santo A, Iervolino I. Seismic soil classification of Italy based on surface geology and shear-wave velocity measurements. Soil Dynam Earthq Eng 2019;122:79–93. https://doi.org/10.1016/j.soildyn.2019.04.002.
[39] Chioccarelli E, Pacifico A, Iervolino I. Italian seismic risk maps based on code-compliant design. Proceedings of the 31st European Safety and Reliability Conference 2021:912–8. https://doi.org/10.3850/978-981-18-2016-8_678-cd.
[40] Chioccarelli E, Cito P, Visini F, Iervolino I. Sequence-based hazard analysis for Italy considering a grid seismic source model. Ann Geophys 2021;64:1–12. https://doi.org/10.4401/ag-8586.
[41] Bindi D, Pacor F, Luzi L, Puglia R, Massa M, Ameri G, et al. Ground motion prediction equations derived from the Italian strong motion database. Bull Earthq Eng 2011;9:1899–920. https://doi.org/10.1007/s10518-011-9313-z.
[42] Beyer K, Bommer JJ. Relationship between median values and between aletory variabilities for different definitions of the horizontal component of motion. Bull Seismol Soc Am 2006;96:1512–22. https://doi.org/10.1785/0120050210.
[43] Kitayama S, Constantinou MC. Collapse performance of seismically isolated buildings designed by the procedures of ASCE/SEI 7. Eng Struct 2018;164:243–58. https://doi.org/10.1016/j.engstruct.2018.03.008.
[44] Cardone D, Perrone G, Piesco V. Developing collapse fragility curves for base-isolated buildings. Earthq Eng Struct Dynam 2019;48:78–102. https://doi.org/10.1002/eqe.3126.